Fermi/Gamma-ray Burst Monitor detection of SGR J1550–5418

Yuki Kaneko and Ersin Göğüş
Sabancı University, Orhanlı-Tuzla, İstanbul 34956, Turkey

Chryssa Kouveliotou
Space Science Office, VP62, NASA/Marshall Space Flight Center, Huntsville, AL 35812, USA

Jonathan Granot
Centre for Astrophysics Research, University of Hertfordshire, College Lane, Hatfield AL10 9AB, UK

Enrico Ramirez-Ruiz
Department of Astronomy and Astrophysics, University of California, Santa Cruz, CA 95064, USA

On behalf of GBM Magnetar Team

SGR J1550–5418 exhibited three active bursting episodes in 2008 October and in 2009 January and March, emitting hundreds of typical Soft Gamma Repeater (SGR) bursts in soft gamma-rays. The second episode was especially intense, and our untriggered burst search on *Fermi*/GBM data (8−1000 keV) revealed ∼450 bursts emitted over 24 hours during the peak of this activity. Using the GBM data, we identified a ∼150-s-long enhanced persistent emission during 2009 January 22 that exhibited intriguing timing and spectral properties: (i) clear pulsations up to ∼110 keV at the spin period of the neutron star, (ii) an additional (to a power-law) blackbody component required for the enhanced emission spectra with $kT \sim 17$ keV, (iii) pulsed fraction that is strongly energy dependent and highest in the 50−74 keV energy band. A total isotropic-equivalent energy emitted during this enhanced emission is estimated to be $2.9 \times 10^{40} (D/5\,\mathrm{kpc})^2$ erg. The estimated area of the blackbody emitting region of $\approx 0.046 (D/5\,\mathrm{kpc})^2$ km^2 is the smallest "hot spot" ever measured for a magnetar and most likely corresponds to the size of magnetically-confined plasma near the neutron star surface.

I. INTRODUCTION

1E 1547.0–5408 was observed with the X-ray Multi-Mirror Mission (XMM-Newton) in 2004 as a magnetar candidate, selected for its galactic plane location and its relatively soft magnetar-like spectrum as seen with the Advanced Satellite for Cosmology and Astrophysics (ASCA) during their Galactic plane survey [1]. Although no period was detected in the original and follow-up XMM observations, its positional coincidence with an extended galactic radio source G327.24-0.13 (possibly a supernova remnant) also suggested that 1E 1547.0–5408 is a magnetar [2]. The subsequent discovery in radio observations of a spin period of 2.07 s and a period derivative of 2.3×10^{-11} s s^{-1} led to an estimated dipole surface field of $B \sim 2.2 \times 10^{14}$ G and confirmed the source's magnetar nature; the source was also renamed as PSR J1550–5418 [3]. Its period makes 1E 1547.0–5408 the fastest rotating magnetar; the source is also one of the only two that emit in radio wavelengths [4, 5]. The distance of the source has been estimated to be ∼4−9 kpc using various methods [2, 3], including the most recent estimate of 4−5 kpc [6]. Throughout this paper we use $D_5 = D/5$ kpc as the source distance measure.

On 2008 October 3, 1E 1547.0–5408 entered an episode of X-ray activity, emitting several typical SGR-like bursts over the next 7 days. During this period, 22 short duration bursts were observed with the Gamma-ray Burst Monitor (GBM) on board the *Fermi* Gamma-ray Space Telescope [7].

The source entered a second period of extremely high X-ray burst activity on 2009 January 22 [8]. During the first 24 hours of this bursting episode, the *Fermi*/GBM triggered on the source 41 times: the number of triggers was limited only by the instrument's capability and did not reflect the actual number of bursts emitted by the source. In fact, our on-ground search for untriggered events revealed a total of ∼450 bursts during this 24 hour period: an unusually high burst frequency from a single source [9]. Based on this SGR-like behaviour, we renamed the source as SGR J1550–5418 [10].

We discovered an enhancement of the persistent emission lasting ∼150 s by examining the data from the first GBM trigger on January 22. Closer inspection of this enhancement in various energy ranges revealed periodic oscillations with a period consistent with the spin period of SGR J1550–5418. Here we present a detailed temporal and spectral analysis of this enhanced emission. In §II, we briefly describe our observations and the GBM instrument and data types. We present our temporal analysis results in §III, and our spectral studies in §IV. Finally we discuss the physical implications of our discovery in §V. Complete descriptions of our analysis and discussion are presented in Kaneko et al. (2010) [11].

II. INSTRUMENTATION AND DATA

In trigger mode, GBM provides three types of data for each of 12 NaI and 2 BGO detectors; CTIME Burst, CSPEC Burst, and Time Tagged Event (TTE) data [12]. The CTIME Burst data have a time resolution of 64 ms with rather coarse spectral information (8 energy channels). The CSPEC Burst data provide high-resolution spectra (128 energy channels) collected every 1.024 s. Both CTIME Burst and CSPEC Burst accumulate data for ∼600 s after a trigger. The TTE data provide time-tagged photon event lists for an accumulation time of 330 s, starting 30 s prior to the trigger time; this data type provides a superior temporal resolution down to 2μs at the same spectral resolution as the CSPEC Burst data.

The first GBM trigger at the onset of the second active episode from SGR J1550–5418 was on 2009 January 22 at 00:53:52.17 UT (= T_0, GBM trigger number 090122037). In the 600 s of the trigger readout we detected many individual short bursts using our on-ground untriggered burst search algorithm. To accept an event as an untriggered burst, we required excess count rates of at least 5.5σ and 4.5σ in the first and second brightest detectors, respectively, in the 10−300 keV energy range. We used CTIME data in both continuous (256 ms time resolution) and Burst mode (64 ms resolution). Subsequently, we inspected energy-resolved burst morphology and compared each detector zenith angle to the source for all 12 detectors, to determine whether the events originated from SGR J1550–5418. In total we identified about a dozen very bright bursts and over 40 less intense bursts within 600 s after T_0 (see Figure 1). During the same trigger readout we also discovered an enhancement in the underlying persistent emission starting at approximately T_0+70 s and lasting for ∼150 s (see inset of Figure 1).

In the analysis presented here, we have exclusively used data from NaI 0, which initially had the smallest detector zenith angle to the source (15°) and to which the source was visible through most of the enhanced emission. We also note that we checked the LAT data (20 MeV−300 GeV) of the entire day for associated high-energy gamma-ray emission, but found no evidence of high-energy photons originating from the direction of SGR J1550–5418.

III. TEMPORAL PROPERTIES

A. Timing Analysis

During our search for untriggered events in the first trigger interval of 2009 January 22 from SGR J1550–5418, we found strong apparent periodic modulations in the enhanced emission period from

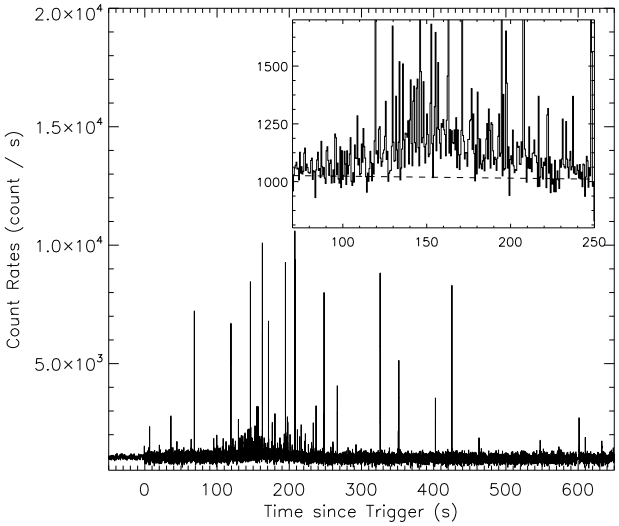

FIG. 1: GBM lightcurve of SGR J1550–5418 in 12−293 keV. An enlarged view of the pulsed, enhanced emission is shown in the inset. The dashed line indicates the background level.

T_0+130 to 160 s in the 50−102 keV data of detector NaI 0 (see panel (c) of Figure 2). This is the first time to our knowledge that pulsations unrelated to a giant flare from a magnetar were clearly seen in the persistent emission of an SGR, in energies up to 100 keV. To search for a coherent pulse period, we performed a timing analysis over the entire enhancement interval. We first eliminated the times of all the bursts found via our untriggered burst search and converted the remaining burst-free intervals to the solar system barycenter. We then generated a Lomb-Scargle periodogram [13, 14] over a range of periods from 0.1 s to 10 s using CTIME Burst data in the 50−102 keV band. We found a very significant signal with a Lomb power of 72.6 (chance occurrence probability, $P_c \simeq 10^{-16}$) at a period of 2.0699 ± 0.0024 s, which is consistent with the spin period of SGR J1550–5418. Further, to confirm our detection, we also employed the $Z^2{}_m$ test (with m = 2) [15] on the burst-free and barycentered TTE data. We find a coherent signal (with a $Z^2{}_{m=2}$ power of 266, $P_c \simeq 10^{-23}$) at the same period. Our spin period measurement is consistent with the one found for SGR J1550–5418 using contemporaneous X-ray data (*Swift*/XRT) [16, 17] and radio data [18]. Therefore, we clearly confirm with the detection of these hard X-ray pulsations that the enhanced persistent emission seen in the inset of Figure 1 originates from SGR J1550–5418.

Next we searched in the enhanced persistent emission for evolution in the intensity of the pulsations using a sliding boxcar technique. We found that the pulsed signal peaks over a 90 s interval, from T_0+120 to 210 s, which encompasses the peak of the enhance-

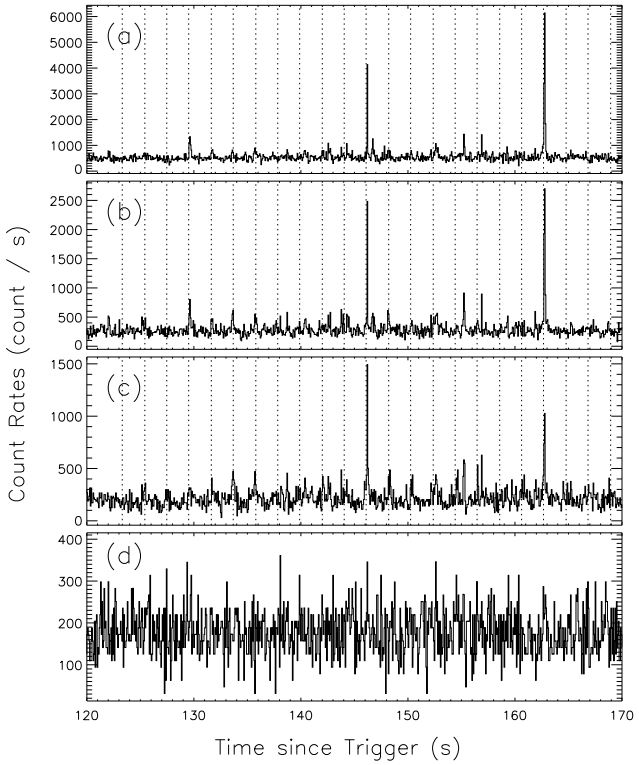

FIG. 2: Lightcurve of SGR J1550–5418 in various energy ranges; (a) 12−27 keV, (b) 27−50 keV, (c) 50−102 keV, and (d) 102−293 keV. The pulsations are most prominent between 50−102 keV (panel c, starting at ∼130 s). The bursts have not been removed here from the data. The dashed lines in panels (a) to (c) indicate the times of the pulse maxima.

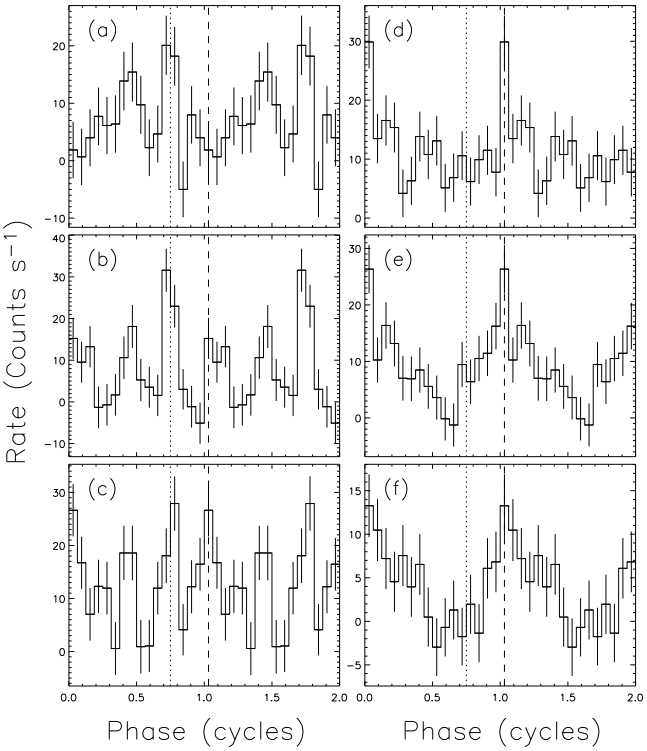

FIG. 3: Pulse profiles of SGR J1550–5418 in equal logarithmic energy intervals; (a) 10−14 keV, (b) 14−22 keV, (c) 22−33 keV, (d) 33−50 keV, (e) 50−74 keV, and (f) 74−110 keV. Two cycles are plotted for clarity. The vertical dotted and dashed lines are explained in §III B.

ment. Finally, we searched for any other intervals exhibiting pulsed emission in the burst-free continuous CTIME data of 2009 January 22 and during the four subsequent days, using a sliding boxcar of 120 s with 10 s steps. We did not find any additional statistically-significant pulsed emission. For the entire search and for all the timing analysis reported here, we used more precise spin ephemeris obtained by contemporaneous *Swift*/XRT, Chandra, XMM-Newton and Suzaku observations [19].

B. Pulse Profiles

To investigate the evolution of the pulse profiles with energy, we folded the burst-free TTE data spanning 120 s (from T_0+100 s to T_0+220 s, which includes the strongest pulsation period as found above) with the spin ephemeris of SGR J1550–5418. We estimated the background level using the data segment between T_0 to T_0+60 s. Figure 3 shows the source pulse profiles during the enhanced emission interval in six energy bands that have the same logarithmic width. The pulse profiles above 110 keV are consistent with random fluctuations, and thus not shown.

Figure 3 indicates that the SGR J1550–5418 pulse profiles in the three lowest energy bands are most likely complex (multi-peaked). While the two lowest energy band profiles are dominated by the structure around phase 0.7-0.8 (indicated by the dotted lines in Figure 3), in the 14−22 keV band we see the emergence of another structure around phase 0.0 (indicated by the dashed lines in Figure 3). This pulse becomes equally prominent in the 22−33 keV range and then dominates in the 33−50 keV band. The pulse profile changes remarkably in the 50-74 keV band, which is the most statistically significant of all the energy bands investigated, and is distinguished by a broad structure that peaks at around phase 0.0. The 74−110 keV profile resembles the 50-74 keV one. As noted above, the pulse profile above 110 keV is consistent with random fluctuations. Therefore, our results set an observed upper energy bound of 110 keV for the hard X-ray pulsations in SGR J1550–5418 during this enhanced emission episode.

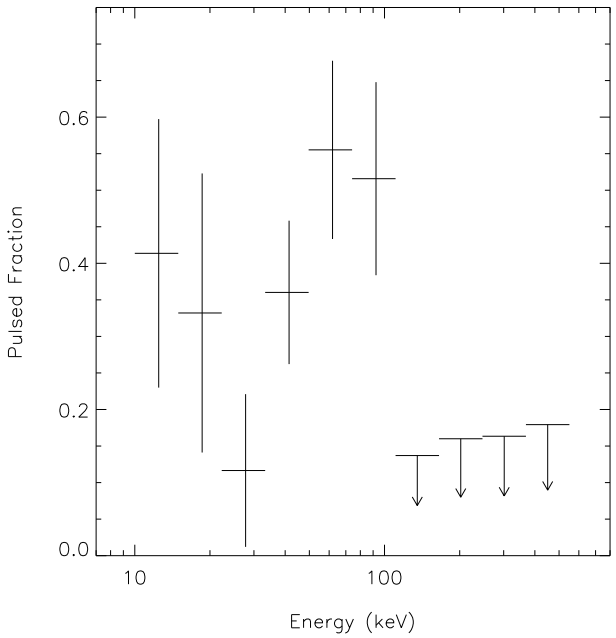

FIG. 4: Evolution of RMS pulsed fraction of SGR J1550–5418 as a function of energy. Uncertainties are 1σ. The energy bands are the same as those used in Figure 3.

C. Pulsed Fraction

We computed the RMS pulsed fraction using a Fourier based approach as described in [20]. In summary, we take the Fourier transform of each pulse profile, then we calculate the RMS pulsed flux by taking the Fourier coefficients of up to third harmonic into account, and finally obtain the pulsed fraction values by dividing the RMS pulsed flux by the phase-averaged flux. In Figure 4, we show the pulsed fraction spectrum of SGR J1550–5418 in the same energy bands as in Figure 3. Although marginally significant, there is an indication of a minimum in the RMS pulsed fraction around ∼30 keV. The RMS reaches its maximum value of 0.55 ± 0.12 in the 50−74 keV band, and then dips below detection at energies greater than ∼110 keV.

IV. SPECTRAL PROPERTIES

A. Time-Integrated and Time-Resolved Spectral Analysis

We analyzed time-integrated and time-resolved spectra of the enhanced emission, using the CSPEC Burst data (8.6−897 keV). Similar to the timing analysis, we excluded all bursts identified with the untriggered search within the enhancement period.

Since the Detector Response Matrices (DRMs) of GBM are time dependent due to the continuous slewing of the spacecraft, a DRM should be generated for every 2-3 degrees of slewing (corresponding to every ∼20−50 s of data). Therefore, we generated DRMs for every 50 s starting from T_0, for this analysis.

We found clear evidence for spectral curvature below 100 keV in the time-integrated spectrum of the entire burst-free enhancement period (72−248 s); a single power law thus resulted in a very poor fit. We employed five other spectral models; cut-off power law, power law + blackbody, optically-thin thermal bremsstrahlung, and single/double blackbody. We found that the time-integrated spectrum is best described by a power law + blackbody (see Figure 5). All other spectral models did not provide better fits mainly because they failed to fit the lower energy excess $\lesssim 10$ keV. The best-fit power-law index and temperature of the additional blackbody are shown in Table I. Adding a blackbody (with $kT = 18 \pm 4$ keV) to a power law resulted in the most significant improvement in Cash statistics [21] over a single power law (ΔC-stat = 13.5 for 2 degrees of freedom, corresponding to an improvement of 3.25σ).

The average energy flux over the entire enhancement is $(6.5 \pm 2.4) \times 10^{-8}\,\mathrm{erg\,cm^{-2}\,s^{-1}}$ (in 8−150 keV), of which the blackbody component accounts for 19%. We estimate a total isotropic emitted energy of $2.9 \times 10^{40} {D_5}^2\,\mathrm{erg}$ for the entire persistent emission (8−150 keV) during the enhancement.

To investigate the evolution of the blackbody component and of the source's spectral properties in general, we divided the enhanced emission period into three time intervals of ∼50 s each: 74−117 s, 122−169 s, and 173−223 s after the trigger time. We employed the same set of photon models as the time-integrated analysis described above. The first spectrum was best fit by a single power law with no evidence of a blackbody or any curvature. The second and third spectra, on the other hand, were best described by power law + blackbody models. In the second spectrum (the peak of the enhancement) the additional blackbody component was statistically most significant, and remained significant in the third spec-

TABLE I: Spectral parameters of the enhanced persistent emission period of SGR J1550–5418. 1-σ uncertainties are shown in parentheses.

Time since T_0 (s)	Power Law Index	Blackbody kT (keV)	Energy Flux* Power Law (10^{-8} ergs/cm^2-s)	Energy Flux* Blackbody (10^{-8} ergs/cm^2-s)
72−248	−2.06 (0.10)	17.7 (3.8)	5.30 (2.37)	1.22 (0.28)
74−117	−2.15 (0.17)	No BB	2.85 (3.30)	–
122−169	−2.09 (0.11)	17.4 (1.7)	7.82 (4.47)	4.08 (0.65)
173−223	−2.14 (0.19)	16.4 (2.7)	5.05 (3.75)	2.59 (0.72)

* Flux is calculated in 8−150 keV.

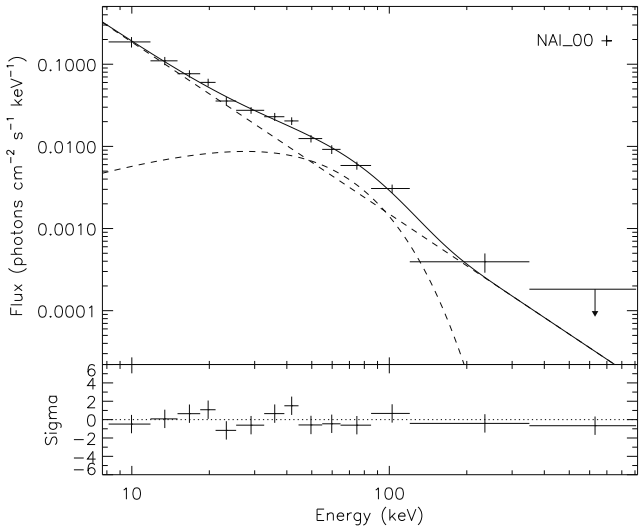

FIG. 5: The photon spectrum of the time interval T_0+122 to 169 s. The blackbody and power-law components are shown separately with dashed curves. The data are binned for display purpose only. A 3σ upper limit is shown for the highest energy bin.

trum as well (ΔC-stat = 42.9 and 15.3, corresponding to 6.2σ and 3.5σ improvements, respectively). The ratio of the blackbody flux to the total flux (8−150 keV) was found to be 34% in both intervals. The indices of the underlying power-law component, and the blackbody temperature also remained constant, at ∼−2.1 and ∼17 keV, respectively (within uncertainties; see also Table 1), while the power-law amplitude tracked the photon flux.

B. Phase-Resolved Spectral Analysis

We performed spin-phase-resolved spectral analysis of the pulsed enhanced emission, as follows: we co-added the burst-free spectrum of each pulse (in T_0+122 to 223 s, corresponding to second and third time-resolved spectra) using TTE data and extracted a phase-maximum spectrum (between phases 0.75−1.25 in Figure 3) and a phase-minimum spectrum (between phases 0.25−0.75). The spin phase for each photon was calculated using barycentered times, as was done for the timing analysis. We calculated the background spectrum, from the burst-free interval at T_0 to T_0+60 s.

The spectra of both the phase minimum and maximum were adequately fitted with power law + blackbody models, where we kept the power-law indices and the blackbody temperatures linked. The values of the linked parameters found in the fit were consistent (within 1σ) with those of the time-integrated spectra (see Table I). The contributions of the blackbody flux to the total flux were (52±18)% and (35±18)%, in the phase-maximum and phase-minimum spectra, respectively. This hints that the blackbody component was more significant in the phase-maximum spectrum than in the phase-minimum spectrum.

V. SUMMARY AND DISCUSSION

We report here the discovery of coherent pulsations in the persistent hard X-ray emission from SGR J1550–5418 in the *Fermi*/GBM data lasting ∼150 s. Coherent pulsations with a 55% RMS pulse fraction have never been detected in the persistent emission at these high energies from a magnetar as yet. These pulsations were detected only at the onset of a major bursting episode and were not directly related to a major burst or flare from the source. Previously, intermediate flares with pulsating tails were observed from SGR 1900+14 [22, 23] and very recently from SGR J1550–5418 (∼6 hours after T_0)[8]. Thermal components were also found in the decaying tails of intermediate events from SGR 1900+14 with much lower blackbody temperatures of ∼2 keV [23]. The thermal component of the enhanced emission we report here is hotter (17 keV), exhibits a strong dependence of the pulse profile with energy with a very high RMS pulsed fraction (up to 55%), and is clearly not associated with a decaying event tail. Energetically, however, the fluence of this enhanced emission is comparable to that of tail emission of the intermediate flares from SGR 1900+14.

Our timing analysis showed that the detection of pulsations is most significant in the 120−210 s interval after trigger. We find that the spectrum requires a blackbody component along with a power law between 122−223 s, which is consistent with the time interval of the most significant detection of pulsations. Moreover, as determined by the energy dependent pulse profiles and RMS pulsed fractions, we find that the high-energy pulsations are most significant in the 50−74 keV range. Strikingly, the blackbody component of the enhanced persistent emission spectrum peaks at around 51 keV (i.e., the Wien peak of 17 keV, see Figure 5). These two independent pieces of evidence lend strong support for a blackbody radiation component to account for the curvature in the spectrum of the enhanced emission.

In our spin-phase-resolved spectral analysis, we find that the blackbody flux to the total emission is (52±18)% and (35±18)% in the phase-maximum and phase-minimum spectra, respectively. This also suggests that a major contribution to the observed pulsations is from the blackbody component. If we assume a surface hot-spot during this pulsating interval, then the best-fit blackbody corresponds to an effective radiating area (as projected on the plane of the sky, far from the star) of $S_\infty = \pi D^2 F/(\sigma T^4) \approx$

$0.046 D_5{}^2$ km^2, where $T \approx 2 \times 10^8$ °K ($kT \approx 17$ keV) is the observed (gravitationally redshifted) temperature. We have used here the blackbody flux at the peak of the pulsations (i.e., phase maximum; $F \approx 5 \times 10^{-8}$ erg cm^{-2} s^{-1}) where the hot-spot is expected to be relatively close to face-on, in order to minimize the effects of projection and gravitational lensing by the neutron star, so that S_∞ would be relatively close to the physical area, S, of the hot spot on the neutron star surface. For a circular hot-spot, this corresponds to a radius of $\sim 120 D_5$ m.

The internal field of magnetars can be significantly stronger and more tangled than the external dipole field. As the internal field twists the stellar crust, the magnetosphere also becomes twisted, possibly in a complex manner [24]. If we identify the inferred size of the hot-spot as the size of a twisted region on the stellar surface, the rate of energy dissipation is expected to be $L_{\rm d} \ll 10^{38}$ erg s^{-1} for global stability case [25]. This is inconsistent with the observed luminosity of the spot, $L_{\rm d} \sim 10^{38} D_5{}^2$ erg s^{-1}

It may be possible for the magnetic twist to grow to a global instability level during a highly active bursting period due to frequent starquakes [25]. As the magnetosphere untwists, a large amount of energy must be dissipated [26]. A small "trapped fireball" – plasma of $e^\pm$ pairs and photons confined by a closed magnetic field region – could then potentially account for the inferred hot-spot, and in particular its roughly constant temperature and size. Confining a "fireball" of energy at least comparable to that emitted by the observed blackbody component, $E_{\rm iso,BB} \approx 5.6 \times 10^{39} D_5{}^2$ erg, within a region of radius $a \sim 120 D_5$ m requires $E_B(a) = \frac{1}{6} a^3 B^2 > E_{\rm iso,BB}$ or $B \gtrsim 1.4 \times 10^{14} D_5^{-1/2}$ G. This is consistent with the surface dipole field of $B \approx 2.2 \times 10^{14}$ G inferred from the measured $P\dot{P}$ [3]. Therefore, a sufficiently small closed magnetic loop anchored by the crust could provide the required confinement. Moreover, the blackbody emission is expected to be accompanied by non-thermal, high-energy radiation produced by collisionless dissipation, with the luminosities comparable to the blackbody components [25]. This is in good agreement with our observations of SGR J1550–5418.

In conclusion, the area of the blackbody emitting region observed here is the smallest "hot spot" measured for a magnetar, which likely arises from magnetically confined hot plasma on the neutron star surface, possibly caused by the gradual dissipative untwisting of the magnetosphere [26]. If the total radiated energy was initially confined to the inferred extremely small size of the enhanced emission region (as in a mini "trapped fireball" scenario), this would indicate a very large magnetic energy density, similar to the "trapped fireball" model for the tails of SGR giant flares. The observed enhanced emission that we report here is much less energetic than a giant flare tail, while its energy is comparable to the tail energy of intermediate events and at the high end of typical SGR bursts. Despite some distinct properties, the enhanced emission of SGR J1550–5418 carries various flavors of all three SGR phenomena, and thus it is most likely related to the very pronounced bursting activity that immediately followed it.

Acknowledgments

This publication is part of the GBM/Magnetar Key Project (NASA grant NNH07ZDA001-GLAST, PI: C. Kouveliotou). We thank G.L. Israel and A. Tiengo for providing the precise spin ephemeris and source distance, respectively, prior to their publication. YK and EG acknowledge EU FP6 Transfer of Knowledge Project "Astrophysics of Neutron Stars" (MTKD-CT-2006-042722). EG acknowledges partial support from Turkish Academy of Sciences. JG gratefully acknowledges a Royal Society Wolfson Research Merit Award. ER-R thanks the Packard Foundation for support.

[1] Sugizaki, M., et al. 2001, ApJs, 134, 77
[2] Gelfand, J.D. & Gaensler, B.M. 2007, ApJ, 667, 1111
[3] Camilo, F., et al. 2007 ApJ, 666, L93
[4] Halpern, J.P., et al. 2005, ApJ, 632, L29
[5] Camilo, F., et al. 2006, Nature, 442, 892
[6] Tiengo, A., et al. 2009, ApJ, in press (arXiv:0911.3064v2)
[7] von Kienlin, A., et al. 2010, in preparation
[8] Mereghetti, S., et al. 2009, ApJ, 696 L74
[9] van der Horst, A.J., et al. 2010, in preparation
[10] Kouveliotou, C., et al. 2009, GCN Circular, 8915
[11] Kaneko, Y., et al. 2010, ApJ, in press (arXiv:0911.4636v2)
[12] Meegan, C., et al. 2009, ApJ, 702, 791
[13] Lomb, N.R. 1975, Ap&SS, 39, 447
[14] Scargle, J.D. 1982, ApJ, 263, 835
[15] Buccheri, R., et al. 1983, A & A, 128, 245
[16] Kuiper, L., den Hartog, P.R., Hermsen, W. 2009, Astron. Tel., 1921
[17] Israel, G.L., et al. 2009, Astron. Tel., 1770
[18] Burgay, M., et al. 2009, Astron. Tel., 1913
[19] Israel, G.L., et al. 2010, in preparation
[20] Woods, P.M., et al. 2007, ApJ, 654, 470
[21] Cash, W. 1979, ApJ, 228, 939
[22] Ibrahim, A.I., et al. 2001, ApJ, 558, 237
[23] Lenters, G.T., et al. 2003, ApJ, 587, 761
[24] Thompson, C., Lyutikov, M., & Kulkarni, S.R. 2002, ApJ, 574, 332

[25] Beloborodov, A.M. & Thompson, C. 2007, ApJ, 657, 967

[26] Lyutikov, M. 2006, MNRAS, 367, 1594